

## A FINITE ELEMENT FORMULATION FOR THE DETECTION OF BOUNDARY CONDITIONS IN ELASTICITY AND HEAT CONDUCTION

B.H. DENNIS and G.S. DULIKRAVICH

*Department of Aerospace Engineering, 233 Hammond Building,  
The Pennsylvania State University, University Park, PA 16802, U.S.A.*

### SUMMARY

A finite element method (FEM) formulation for the detection of unknown steady boundary conditions in heat conduction and linear elasticity continuum problems is presented. The present FEM is capable of determining displacements, surface stresses, temperatures, and heat fluxes on the boundaries where such quantities are unknown or inaccessible, provided such quantities are sufficiently over-specified on other boundaries. Details of the discretization, linear system solution techniques, and sample results for 2-D and 3-D problems are presented.

### KEYWORDS

Finite elements, ill-conditioned matrices, inverse boundary conditions, elasticity, heat conduction.

### FINITE ELEMENT FORMULATIONS

The Navier equations for linear static deformations  $u, v, w$  in three-dimensional Cartesian  $x, y, z$  coordinates are

$$(\lambda + G) \left( \frac{\partial^2 u}{\partial x^2} + \frac{\partial^2 v}{\partial x \partial y} + \frac{\partial^2 w}{\partial x \partial z} \right) + G \nabla^2 u + X = 0 \quad (1)$$

$$(\lambda + G) \left( \frac{\partial^2 u}{\partial x \partial y} + \frac{\partial^2 v}{\partial y^2} + \frac{\partial^2 w}{\partial y \partial z} \right) + G \nabla^2 v + Y = 0 \quad (2)$$

$$(\lambda + G) \left( \frac{\partial^2 u}{\partial x \partial z} + \frac{\partial^2 v}{\partial y \partial z} + \frac{\partial^2 w}{\partial z^2} \right) + G \nabla^2 w + Z = 0 \quad (3)$$

where  $E$  is the Young's modulus of elasticity and  $\nu$  is the Poisson's ratio so that

$$\lambda = \frac{E\nu}{(1+\nu)(1-2\nu)}, G = \frac{E}{2(1+\nu)}$$

The terms  $X, Y, Z$  are body forces per unit volume due to gravity and thermal loading.

$$X = -\rho g_x - (3\lambda + 2G) \frac{\partial \alpha \Delta T}{\partial x} \quad (4)$$

$$Y = -\rho g_y - (3\lambda + 2G) \frac{\partial \alpha \Delta T}{\partial y} \quad (5)$$

$$Z = -\rho g_z - (3\lambda + 2G) \frac{\partial \alpha \Delta T}{\partial z} \quad (6)$$

The term  $\Delta T$  is the difference between the local temperature and a reference temperature,  $T_0$ . This system of differential equations can be written in the following matrix form

$$[L]^T ([C][L]\{\delta\} - [C]\{\varepsilon_0\}) - \{f_b\} = 0 \quad (7)$$

where the differential operator matrix,  $L$ , is defined as

$$[L] = \begin{bmatrix} \frac{\partial}{\partial x} & 0 & 0 \\ 0 & \frac{\partial}{\partial y} & 0 \\ 0 & 0 & \frac{\partial}{\partial z} \\ \frac{\partial}{\partial y} & \frac{\partial}{\partial x} & 0 \\ \frac{\partial}{\partial z} & 0 & \frac{\partial}{\partial x} \\ 0 & \frac{\partial}{\partial z} & \frac{\partial}{\partial y} \end{bmatrix} \quad (8)$$

and the elastic modulus matrix,  $C$ , is defined as

$$[C] = \frac{E}{(1+\nu)(1-2\nu)} \begin{bmatrix} 1-\nu & \nu & \nu & 0 & 0 & 0 \\ \nu & 1-\nu & \nu & 0 & 0 & 0 \\ \nu & \nu & 1-\nu & 0 & 0 & 0 \\ 0 & 0 & 0 & \frac{1-2\nu}{2} & 0 & 0 \\ 0 & 0 & 0 & 0 & \frac{1-2\nu}{2} & 0 \\ 0 & 0 & 0 & 0 & 0 & \frac{1-2\nu}{2} \end{bmatrix} \quad (9)$$

Casting the system of equations (7) in integral form using the weighted residual method yields

$$\int_{\Omega} [V][L]^T ([C][L]\{\delta\} - [C]\{\epsilon_0\}) d\Omega - \int_{\Omega} [V]\{f_b\} d\Omega = 0 \quad (10)$$

where the matrix,  $V$ , is the weight matrix which is a collection of test functions.

$$[V] = \begin{bmatrix} v_1 & 0 & 0 \\ 0 & v_2 & 0 \\ 0 & 0 & v_3 \end{bmatrix} \quad (11)$$

One should now integrate (10) by parts to get the weak form of (7)

$$\int_{\Omega} ([L][V]^T)^T [C][L]\{\delta\} d\Omega - \int_{\Omega} ([L][V]^T)^T [C]\{\epsilon_0\} d\Omega - \int_{\Omega} [V]\{f_b\} d\Omega - \int_{\Gamma_1} [V]\{T\} d\Gamma = 0 \quad (12)$$

where  $T$  is the vector of surface tractions on surface  $\Gamma_1$ .

$$\{T\} = [n][C][L]\{\delta\} \quad (13)$$

The matrix  $[n]$  contains the Cartesian components of the unit vector normal to the surface  $\Gamma_1$ . The displacement field in the  $x$ ,  $y$ , and  $z$  directions can now be approximated with approximation functions

$$\delta_x(x, y, z) \approx \bar{\delta}_x^e(x, y, z) = \sum_{i=1}^n N_i(x, y, z) u_i \quad (14)$$

$$\delta_y(x, y, z) \approx \bar{\delta}_y^e(x, y, z) = \sum_{i=1}^n N_i(x, y, z) v_i \quad (15)$$

$$\delta_z(x, y, z) \approx \bar{\delta}_z^e(x, y, z) = \sum_{i=1}^n N_i(x, y, z) w_i \quad (16)$$

Equations (14)-(16) can be rewritten in matrix form

$$\{\tilde{\delta}^e\} = [N]\{\delta^e\} \quad (17)$$

(8) where  $N$  is the interpolation matrix which contains the trial functions for each equation in the system. Also note that with Galerkin's method the weight matrix and the interpolation matrix are equal,  $N = V^T$ . If the matrix  $B$  is defined as

$$[B] = [L][N] \quad (18)$$

then the substitution of the approximation functions (17) into the weak statement (12) creates the weak integral form for a finite element expressed as

$$(9) \quad \int_{\Omega^e} [B]^T [C] [B] \{\delta^e\} d\Omega^e - \int_{\Omega^e} [B]^T [C] \{\varepsilon_0^e\} d\Omega^e - \int_{\Omega^e} [N]^T \{f_b^e\} d\Omega^e - \int_{\Gamma_1^e} [N]^T \{T^e\} d\Gamma^e = 0 \quad (19)$$

This can also be written in the matrix form as

$$[K^e]\{\delta^e\} = \{f^e\} \quad (20)$$

For thermal stresses, the initial elemental strain vector,  $\varepsilon_0^e$ , becomes

$$\{\varepsilon_0^e\} = \left[ \alpha \Delta T(x, y, z) \quad \alpha \Delta T(x, y, z) \quad \alpha \Delta T(x, y, z) \quad 0 \quad 0 \quad 0 \right]^T \quad (21)$$

For gravitational body forces, the elemental body force vector,  $f_b^e$ , becomes

$$(11) \quad \{f_b^e\} = \left[ \rho g_x \quad \rho g_y \quad \rho g_z \quad 0 \quad 0 \quad 0 \right]^T \quad (22)$$

The local stiffness matrix,  $K^e$ , and the force vector,  $f^e$ , are determined for each element in the domain and then assembled into the global system

$$[K]\{u\} = \{F\} \quad (23)$$

(12) The global displacements are found by solving this system of linear algebraic equations. The stresses,  $\sigma$ , can then be found in terms of the displacements,  $\delta$

$$\{\sigma\} = [C][L]\{\delta\} - [C]\{\varepsilon_0\} \quad (24)$$

(13) The temperature distribution throughout the domain can be found by solving Poisson's equation for steady linear heat conduction with a distributed steady heat source function,  $Q$ , and thermal conductivity coefficient,  $k$ .

$$-k \left( \frac{\partial^2 T}{\partial x^2} + \frac{\partial^2 T}{\partial y^2} + \frac{\partial^2 T}{\partial z^2} \right) = Q \quad (25)$$

(14) Applying the method of weighted residuals to (25) over an element results in

$$(15) \quad \int_{\Omega^e} \left( \frac{\partial^2 T}{\partial x^2} + \frac{\partial^2 T}{\partial y^2} + \frac{\partial^2 T}{\partial z^2} - \frac{Q}{k} \right) v d\Omega^e = 0 \quad (26)$$

(16) Integrating this by parts once (26) creates the weak statement for an element

$$- \int_{\Omega^e} k \left( \frac{\partial v}{\partial x} \frac{\partial T}{\partial x} + \frac{\partial v}{\partial y} \frac{\partial T}{\partial y} + \frac{\partial v}{\partial z} \frac{\partial T}{\partial z} \right) d\Omega^e = \int_{\Omega^e} N_i Q d\Omega^e - \int_{\Gamma^e} N_i (q \cdot \hat{n}) d\Omega^e \quad (27)$$

Variation of the temperature across an element can be expressed by

$$T(x, y, z) \approx \tilde{T}^e(x, y, z) = \sum_{i=1}^m N_i(x, y, z) T_i \quad (28)$$

Using Galerkin's method, the weight function  $v$  and the interpolation function for  $T$  are chosen to be the same.

By defining the matrix  $B$  as

$$[B] = \begin{bmatrix} \frac{\partial N_1}{\partial x} & \frac{\partial N_2}{\partial x} & \dots & \frac{\partial N_m}{\partial x} \\ \frac{\partial N_1}{\partial y} & \frac{\partial N_2}{\partial y} & \dots & \frac{\partial N_m}{\partial y} \\ \frac{\partial N_1}{\partial z} & \frac{\partial N_2}{\partial z} & \dots & \frac{\partial N_m}{\partial z} \end{bmatrix} \quad (29)$$

the weak statement (27) can be written in the matrix form as

$$[K_c^e]\{T^e\} = \{Q^e\} \quad (30)$$

where

$$[K_c^e] = \int_{\Omega^e} k [B]^T [B] d\Omega^e \quad (31)$$

$$\{Q^e\} = - \int_{\Omega^e} Q \{N\} d\Omega + \int_{\Gamma^e} q_s \{N\} d\Gamma^e \quad (32)$$

$$(33)$$

The local stiffness matrix,  $K_c^e$ , and heat flux vector,  $Q^e$ , are determined for each element in the domain and then assembled into the global system

$$[K_c]\{T\} = \{Q\} \quad (34)$$

The above equations for steady heat conduction and linear elasticity were discretized separately by using a Galerkin's finite element method. This results in two linear systems of algebraic equations

$$[K]\{U\} = \{F\}, \quad [K_c]\{T\} = \{Q\} \quad (35)$$

These systems are large, sparse, symmetric, and positive definite. Once these global systems have been formed, the boundary conditions can be applied. For a well-posed analysis (direct) problem, the boundary conditions must be known on all boundaries of the domain. For heat conduction, either the temperature,  $T_s$ , or the heat flux,  $Q_s$ , must be specified at each point of the boundary. For elasticity, the displacement vector components,  $U_s, V_s, W_s$ , or the surface traction vector components,  $T_{xs}, T_{ys}, T_{zs}$ , must be specified on the entire boundary.

For inverse problems, the unknown boundary conditions on parts of the boundary can be determined by over-specifying the boundary conditions (enforcing both Dirichlet and Neumann type boundary conditions) on at least some of the remaining portions of the boundary, and providing either Dirichlet or Neumann type boundary conditions on the rest of the boundary. It is possible, after a series of algebraic manipulations, to transform the original system of equations into a system which enforces the over-specified boundary conditions and includes the unknown boundary conditions as a part of the unknown solution vector. This formulation is an adaptation of a method by Martin and Dulikravich [1] for the inverse detection of boundary conditions in steady heat conduction and by Martin, Halderman and Dulikravich in elastostatics [2] using the boundary element method (BEM).

As an example, consider the linear system for heat conduction on a quadrilateral finite element with boundary conditions given at points 1 and 4.

$$(28) \quad \begin{bmatrix} K_{11} & K_{12} & K_{13} & K_{14} \\ K_{21} & K_{22} & K_{23} & K_{24} \\ K_{31} & K_{32} & K_{33} & K_{34} \\ K_{41} & K_{42} & K_{43} & K_{44} \end{bmatrix} \begin{Bmatrix} T_1 \\ T_2 \\ T_3 \\ T_4 \end{Bmatrix} = \begin{Bmatrix} Q_1 \\ Q_2 \\ Q_3 \\ Q_4 \end{Bmatrix} \quad (36)$$

As an example of an inverse problem, one could specify both the temperature,  $T_s$ , and the heat flux,  $Q_s$ , at point 1, flux only at points 2 and 3, and assume the boundary conditions at point 4 as being unknown. The original system of equations (36) can be modified by adding a row and a column corresponding to the additional equation for the over-specified flux at point 1 and the additional unknown due to the unknown boundary flux at point 4.

$$(30) \quad \begin{bmatrix} 1 & 0 & 0 & 0 & 0 \\ K_{21} & K_{22} & K_{23} & K_{24} & 0 \\ K_{31} & K_{32} & K_{33} & K_{34} & 0 \\ K_{41} & K_{42} & K_{43} & K_{44} & -1 \\ K_{11} & K_{12} & K_{13} & K_{14} & 0 \end{bmatrix} \begin{Bmatrix} T_1 \\ T_2 \\ T_3 \\ T_4 \\ Q_4 \end{Bmatrix} = \begin{Bmatrix} T_s \\ Q_2 \\ Q_3 \\ 0 \\ Q_s \end{Bmatrix} \quad (37)$$

The same procedure can be applied to the system matrices for both heat conduction and elasticity in 2-D or 3-D. The resulting systems of equations will remain sparse, but will become unsymmetrical and possibly rectangular depending on the ratio of the number of known to unknown boundary conditions. The next section will discuss techniques for solving such systems.

## SOLUTION OF THE LINEAR SYSTEM

In general, the resulting FEM systems for the inverse thermoelastic problems are sparse, unsymmetrical, and often rectangular instead of square. These properties make the process of finding a solution to the system very challenging. Three approaches will be discussed here.

The first is to normalize the equations by multiplying both sides by the matrix transpose and solve the resulting square system with common sparse solvers.

$$(35) \quad [K]^T [K] \{U\} = [K]^T \{F\} \quad (38)$$

This approach has been found to be effective for certain inverse problems [3]. The resulting normalized system is much less sparse than the original system, but it is square, symmetric, and positive definite. The normalized system is solved with a direct method (Cholesky or LU factorization) or with an iterative method (preconditioned Krylov subspace). There are several disadvantages to this approach. Among them being the computation expense of computing  $[K]^T [K]$ , the large incore memory requirements, and the roundoff error incurred during the  $[K]^T [K]$  multiplication.

A second approach is to use iterative methods suitable for unsymmetrical and least squares problems. One such method is the LSQR method, which is an extension of the well-known conjugate gradient method [4]. The LSQR method and other similar methods such as the least squared conjugate gradient (CGLS) solve the normalized system, but without explicit computation of  $[K]^T [K]$ . However, convergence rate of these methods depend strongly on the condition number of the normalized system which is roughly the condition number of  $[K]$  squared. Convergence can be slow when solving the ill-conditioned systems resulting from the inverse finite element discretization.

A third approach is to use a non-iterative method for unsymmetrical and least squares problems such as QR factorization or SVD [5]. However, sparse implementations of QR or SVD solvers are needed to make the incore memory requirements reasonable for the inverse finite element problems.

## NUMERICAL RESULTS

The accuracy and efficiency of the finite element inverse formulation was tested on several simple 2-D problems with known analytic solutions. The method was implemented in an object-oriented finite element code written in C++. Elements used in the calculations were triangles with linear and quadratic interpolation functions. The triangular meshes were generated by an automatic Delauney triangulation technique [6]. Three different solution techniques were tested: a sparse QR factorization [7], a CGLS code, and a CG solver applied to solving the normalized equations. Several 2-D problems with analytical solutions were used to test the accuracy of FEM numerical solutions of direct and inverse problems in both heat conduction and linear elasticity. The three basic test geometries included a rectangular plate, an annular disk (Fig. 1), and a rectangular plate with two rectangular holes (Fig. 3).

For heat conduction, one analytical test problem consisted of a rectangular homogeneous plate with uniform temperatures specified at the opposite boundaries and adiabatic conditions specified at the remaining two opposite boundaries. The FEM solution of this direct problem was less than 1% in error. An inverse boundary condition determination problem was then created by over-specifying the boundary conditions (specifying both the temperatures and the fluxes) at one end of the plate while specifying nothing at the opposite end of the plate and keeping the adiabatic conditions on the side walls. This numerical solution also had less than 1% error when compared to the analytical solution. Another simple test case was steady heat conduction in an annular homogeneous disk (Fig. 1). In a direct (well-posed) problem a uniform temperature of 50.0 K was enforced on the inner circular boundary while a temperature of 10.0 K was enforced on the outer circular boundary. The temperature field (Fig. 4) computed with the FEM had a maximum error of 1% compared to the analytical solution. The inverse problem was created by overspecifying on the outer circular boundary the temperatures and fluxes while providing no boundary conditions on the inner circular boundary [1]. The temperature distribution predicted by the inverse version of the FEM code had a maximum error of 3% (Fig. 5) when compared to the analytical solution (Fig. 4).

For elasticity, one analytical test problem consisted of a rectangular homogeneous plate under uniform tension at one end while having a fixed opposite boundary and zero tractions on the side walls. The FEM solution of this direct (well-posed) problem was less than 1% in error. An ill-posed problem was then created by specifying both the displacements and tractions at one end and nothing at the other end of the plate while enforcing zero tractions on the side walls. The FEM solution of this inverse (ill-posed) problem also had less than 1% relative error when compared with the analytical solution. Another elasticity test case was also utilized where an annular pressure vessel was used to test the FEM code [2]. The FEM solution of a well-posed (direct or analysis) problem was obtained when specifying tractions on both the inner and the outer circular boundaries. The computed stress distributions (Figs. 7, 6, 10) were less than 2% in error. An inverse (ill-posed) problem was then generated by overspecifying the displacements and tractions on the outer circular boundary while providing no boundary conditions on the inner circular boundary. The FEM predicted the stress and deformation fields (Figs. 9, 8, 2) that had a maximum error of 4% for stresses and 2% for deformations compared to the analytical solution.

A heat conduction problem in a multiply-connected domain (Fig. 3) was also numerically tested. The well-posed problem used a constant temperature of 50.0 K on the walls of the two rectangular holes while enforcing a constant temperature of 10.0 K on the outer rectangular boundary. Thermal conductivity was  $k = 1 \text{ Wm}^{-1}\text{K}^{-1}$  and a uniform heat source was  $Q = 1000.0 \text{ Wm}^{-3}$ . For the ill-posed problem, the temperatures and fluxes from the FEM solution of the well-posed problem were enforced on the outer boundary while nothing was specified on the rectangular holes. The resulting

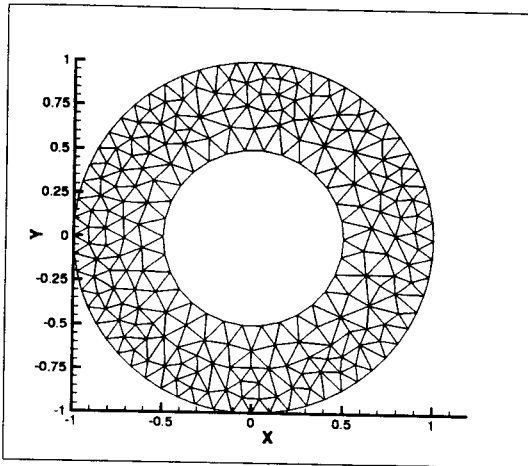


Figure 1: Triangular mesh for an annular disk test case geometry

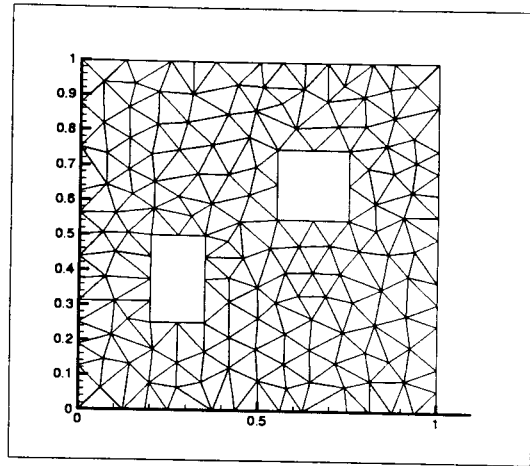


Figure 2: Triangular mesh for a multiply-connected domain test case geometry

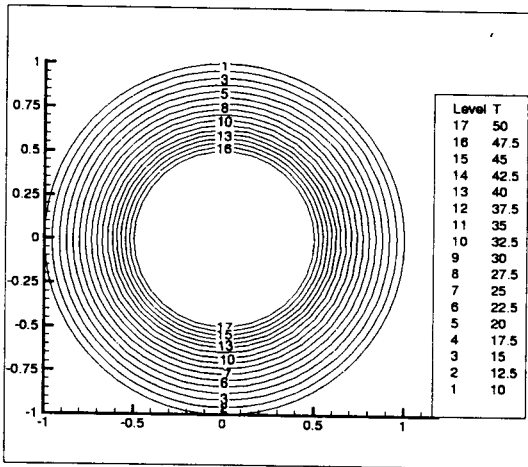


Figure 3: Computed isotherms with inner and outer boundary temperatures specified

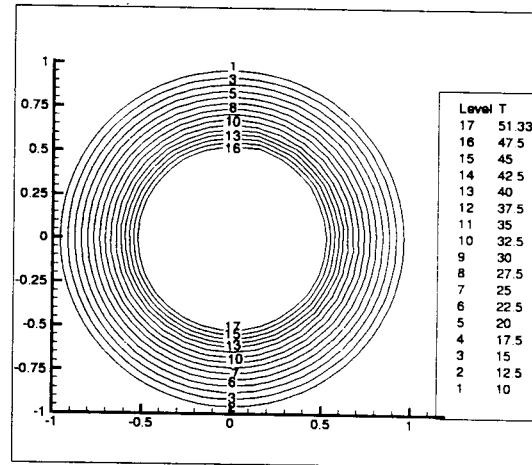


Figure 4: Computed isotherms with outer boundary temperatures and fluxes specified

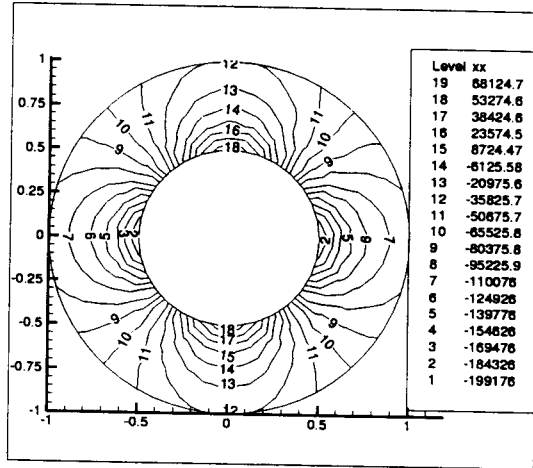


Figure 5: Computed axial stress distribution with inner and outer boundary tractions specified

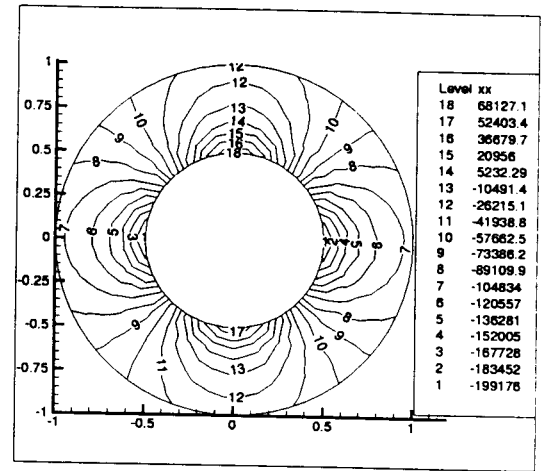


Figure 6: Computed axial stress distribution with outer boundary tractions and displacements specified

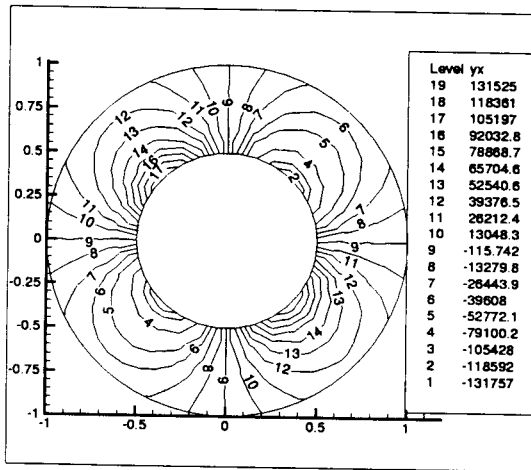


Figure 7: Computed shear stress distribution with inner and outer boundary tractions specified

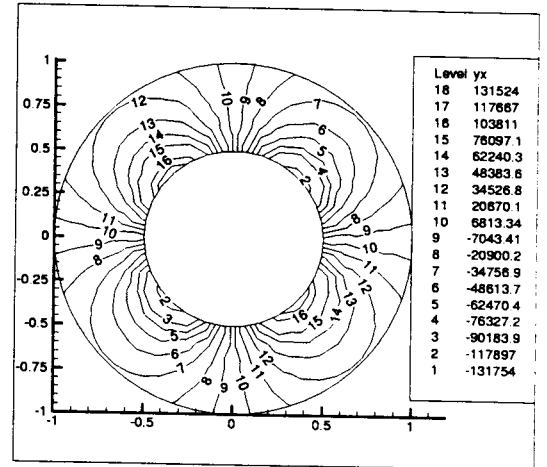


Figure 8: Computed shear stress distribution with inner and outer boundary tractions and displacements specified



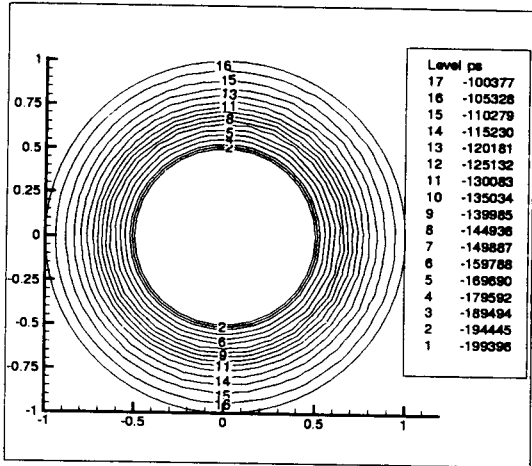


Figure 9: Computed principle stress distribution with inner and outer boundary tractions specified

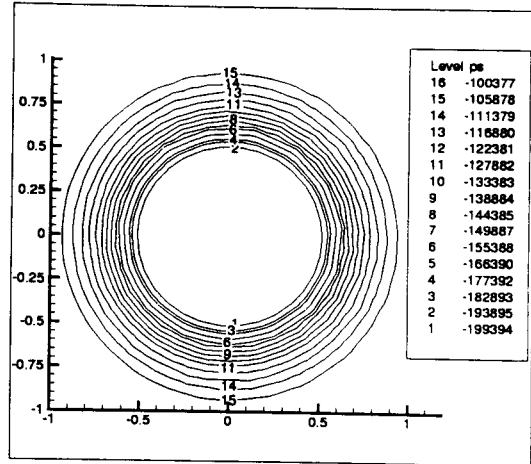


Figure 10: Computed principle stress distribution with inner and outer boundary tractions and displacements specified

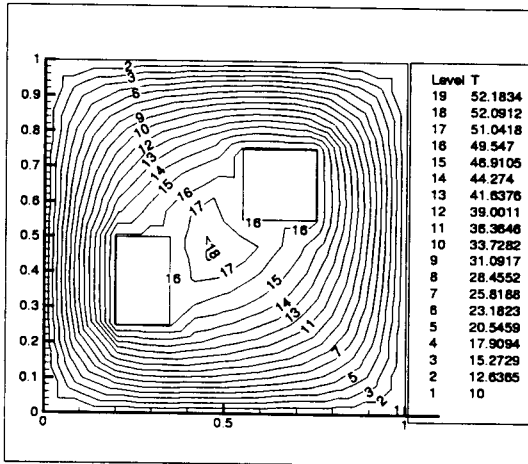


Figure 11: Computed isotherms for inner and outer boundary temperatures specified

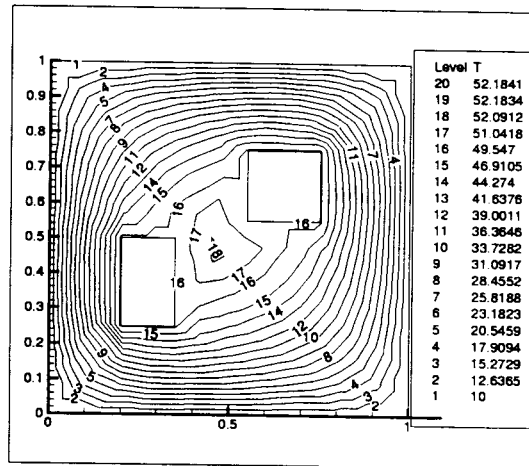


Figure 12: Computed isotherms for outer boundary temperatures and fluxes specified

temperature distributions for both the well-posed and the ill-posed problems show good agreement (Figs. 11, 12) with a maximum relative difference between the two solutions of 2%.

All three sparse solvers performed well for test cases with relatively small number of variables. The QR factorization was found to provide the highest accuracy in the shortest amount of computing time. For each of the test problems presented here the total solution time was less than 1 second on a Pentium 200 MHz PC. However, the QR factorization failed for larger problems where the number of grid points was greater than about 2000. This is most likely due to the instability of the QR algorithm when dealing with systems with high condition numbers [5]. The CG method applied to the normalized equations worked well for problems with less than 100 nodes. For more than 100 nodes, this method required many iterations to converge to a solution less accurate than the QR solution. The CGLS method was found to be slow for problems with more than 500 nodes, but was able to provide accurate solutions for problems where the QR factorization broke down.

### ACKNOWLEDGMENTS

The authors are grateful for the National Science Foundation Grant DMI-9522854 monitored by Dr. George Hazelrigg, the NASA Lewis Research Center Grant NAG3-1995 facilitated by Dr. John Lytle and supervised by Dr. Kestutis Civinskas, and for ALCOA Foundation Faculty Research Award facilitated by Dr. Yimin Ruan.

### References

- [1] Martin, T. J. and Dulikravich, G. S. (August 1996) *ASME Journal of Heat Transfer*, Vol. 118, No. 3, pp. 546-554.
- [2] Martin, T. J., Halderman, J. and Dulikravich, G. S. (September 1995) *Computers and Structures*, Vol. 56, No. 5, pp. 825-836.
- [3] Boschi, L. and Fischer, R. P. (1996) Iterative solutions for tomographic inverse problems: LSQR and SIRT, Technical Report, Seismology, Harvard University, Cambridge, MA.
- [4] Paige, C. C. and Saunders, M. A. (1982) *ACM Transactions on Mathematical Software*, Vol. 8, No. 1, pp. 43-71.
- [5] Golub, G. H. and Van Loan, C. F. (1996) *Matrix Computations*, Johns Hopkins, Baltimore, MD.
- [6] Shewchuk, J. R. (May 1996) Triangle: Engineering a 2D Quality Mesh Generator and Delaunay Triangulator, First Workshop on Applied Computational Geometry, Philadelphia, PA.
- [7] Matstoms, P. (1991) The multifrontal solution of sparse least squares problems. Licentiat thesis, Department of Mathematics, Linköping University, Sweden

# INVERSE PROBLEMS IN ENGINEERING MECHANICS

---

International Symposium on Inverse Problems  
in Engineering Mechanics 1998 (ISIP '98)  
Nagano, Japan

*Editors*

**M. Tanaka**

Department of Mechanical Systems Engineering  
Shinshu University, 500 Wakasato, Nagano 380-8553  
Japan

**G.S. Dulikravich**

Department of Aerospace Engineering  
The Pennsylvania State University, University Park  
PA 16802, USA



1998

**ELSEVIER**

Amsterdam · Lausanne · New York · Oxford · Shannon · Singapore · Tokyo